The evolution of wingtip vortex wandering – A stability analysis based on stereo PIV experiment

Siyi Qiu, Yang Xiang, Hong Liu

J. C. Wu Center for Aerodynamics

School of Aeronautics and Astronautics

Shanghai Jiao Tong University

leon-the-chosy@sjtu.edu.cn; xiangyang@sjtu.edu.cn; hongliu@sjtu.edu.cn

Abstract Instability, as a potential mechanism for vortex flow control, is manifested typically in the phenomenon of wingtip vortex wandering. In this paper, the evolution of wingtip vortex generated by a NACA0015 rectangular wing within 6 chord lengths of its wake at Re=2.1×10^5-3.5×10^5 and *AoA* = 4°- 10°is investigated by stereo particle image velocimetry experiment. The streamwise evolution of vortex wandering is clearly captured which demonstrates strong anisotropy. The amplitude of vortex wandering increases on all conditions, which exhibits greater growth rates in the condition of larger *AoA*. To account for such phenomenon, spatial linear stability analysis is performed on the base flow obtained by SPIV experiment to investigate quantitatively the amplification of small disturbance and disturbance modes at the experiment conditions. It is discovered that the wingtip vortex in the experiment is marginally stable in all conditions. Furthermore, the spatial growth rates of instability by *AoA* correspond well with that of wandering amplitude, indicating that the quick enlargement of the amplitude of wandering at larger *AoA* condition is caused by a higher level of instability. In addition, the least-stable disturbance mode by LSA reveals a non-zero directed velocity perturbation in the vortex core which rotates periodically. Such perturbation developing in both time and space, which is stirred by vortex instability, leads to the behavior of wingtip vortex wandering.

Keywords *wingtip vortex, SPIV, linear stability analysis, vortex instability*

1 Introduction

The wingtip vortex is a typical large-scale vortex structure in the wake of aircraft, which can maintain for up to 100 times the chord-length, threatening the flight safety of following aircrafts and limits the airport capacity. In addition, the induced drag generated by wingtip vortex is one of the main sources of aircraft resistance [1]. Therefore, Gerz proposed two strategies to alleviate the influence of aircraft trailing vortices: 1. Low Vorticity Vortex, 2. Quickly Decaying Vortex [2]. The circulation of wingtip vortex has been reduced effectively by facilitating wingtip devices, while for the second strategy, there has been no effective flow control principles and methods. In fact, studies have shown that vortex breakdown is closely

related to its instability characteristics [3], and wingtip vortex manifests evident properties of instability during its evolution. Researchers have discovered that the wingtip vortex generally demonstrates a low-frequency wandering behavior which has been proved to be caused by the inherent instability of wingtip vortex [4]. In addition, such wandering behavior possess a dominate frequency throughout its wake [5]. A potential flow control method can therefore be proposed to accelerate the decaying of wingtip vortex by matching the dominant frequency of the external actuation and the base flow or utilizing the long-wave or short-wave instability to amplify the growth rate of disturbance. Therefore, by investigating the wandering behavior of wingtip vortex, the mechanism of instability and its effect on wingtip vortex can be accounted, which can further guide the input excitation mode by the disturbance mode or frequency of instability.

Vortex wandering is a typical phenomenon of wingtip vortex by the effect of its inherent instability, which demonstrates a low-frequency fluctuation motion in the streamwise plane [6]. Due to its 'blurring' effect on the measurement of wingtip vortex, early researches mainly focused on its correction by means of deconvolution and vortex re-centering. The instantaneous vortex center was found to conform with Gaussian distribution and displayed anisotropic feature [7]. The amplitude of wandering was shown to grow in the streamwise direction, and decrease with increasing angle of attack [8], and therefore decrease with circulation of the vortex [9]. In Edstrand's work[4], leading modes extracted from PIV-obtained flow field and most unstable modes by linear stability analysis of a fitted Batchelor vortex were compared and found to be identical, which confirmed that the origin of wandering was its instability. In short, there have been effective methods to correct the side-effect of vortex wandering, and instability has been taken as one of its primary factors at present. However, the mechanism underlying the spatial evolution of such wandering motion hasn't been fully understood, which requires further investigation.

Linear stability analysis (LSA) linearizes small disturbances in a basic flow configuration and solve its spatial/temporal growth/damping rate, frequency/wavenumber and disturbance mode quantitatively [10], which exactly suits the problem studied herein. Previous efforts include studies of the effect of Reynolds number, swirl parameter and azimuthal wavenumber on the stability of a theoretical Batchelor vortex[11][12]. In Oberleithner's stability analysis of a swirling jets, a global resonant frequency was found throughout the wake [13] and Bi-global LSA performed by Edstrand *et al.* tackled the influence of trailing wake on the stability of wingtip vortex solved by DNS computation at Re=1000 [14]. However, the temporal and spatial evolution of the instability of wingtip vortex has not been fully investigated, which limits the knowledge of the underlying mechanism of vortex wandering and its development. Therefore, in this paper, linear stability analysis is performed to obtain the growth rate and also the most unstable mode of small disturbance in the wingtip vortex flow throughout the wake region covered by Stereo-PIV experiment, so as to quantify the effect of instability on the wingtip vortex flow and also on the spatial development of vortex wandering.

Fig. 1 Stereo-PIV experimental setup

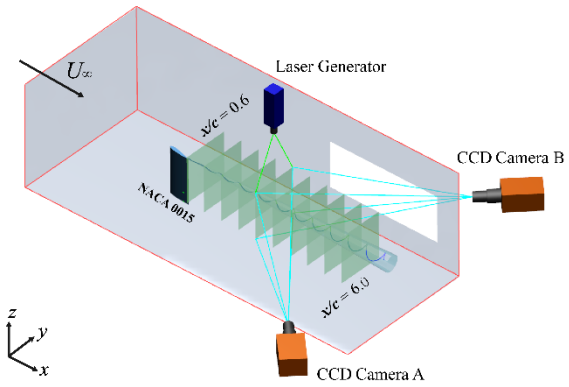

2 Experimental setup and data processing

2.1 SPIV experiment setup

The experiment is conducted in the low-speed tunnel in Shanghai Jiao Tong University with an experimental section of 1200mm×900mm, with the turbulence level of test section measured to be 0.2%. A NACA0015 rectangular wing with chord length of c = 0.203 m and an aspect ratio of 2.0 was used to generate the wingtip vortex. Four angle of attack AoA = 4°, 8°, and 10° and three wind speed conditions of 15m/s, 20m/s, and 25m/s is tested in the experiment, corresponding to Re = 2.1×10^5, 2.8×10^5, and 3.5×10^5, adding up to a total of 9 conditions. In addition, the wingtip vortex flow with different cross-sections in the wake is measured for each condition. The measurement range is x/c = 0.6 - 6.0.

The wing-tip vortex field was obtained by SPIV. The double-pulse energy of the laser is 2×200 mJ, and the double-pulse frequency is 1 Hz, with the interval between two pulses is 10 ms. The thickness of the plane light source is 2 mm and two high-resolution CCD cameras, the angle between which being 90 degrees were used to record the trace of particles, as shown in Fig.1. 200 snapshots are recorded at a frequency of 1 Hz.

2.2 Data post-processing

The 3-dimensional vector field is processed by INSIGHT 4G commercial software with an interrogation window of 24×24 pixels, yielding a resolution of 0.89 mm/grid. The vorticity and each related parameter are then calculated by the three components of velocity u, v, w.

The instantaneous location of vortex center is obtained by using the first moment of streamwise vorticity ω_x, as defined in Eq. 1, which minimizes the blurring effect of vortex wandering. The wandering amplitude is represented by the standard deviation $\sigma = \sqrt{\sigma_y^2 + \sigma_z^2}$ of instantaneous vortex center, and the correlation of wandering motion in y- and z- direction is determined by $e(y,z) = \mathrm{cov}(y,z)/(\sigma_y\sigma_z)$.

$$y_c = \frac{\iint y\omega_x(y,z)dydz}{\iint \omega_x(y,z)dydz},\ z_c = \frac{\iint z\omega_x(y,z)dydz}{\iint \omega_x(y,z)dydz} \tag{1}$$

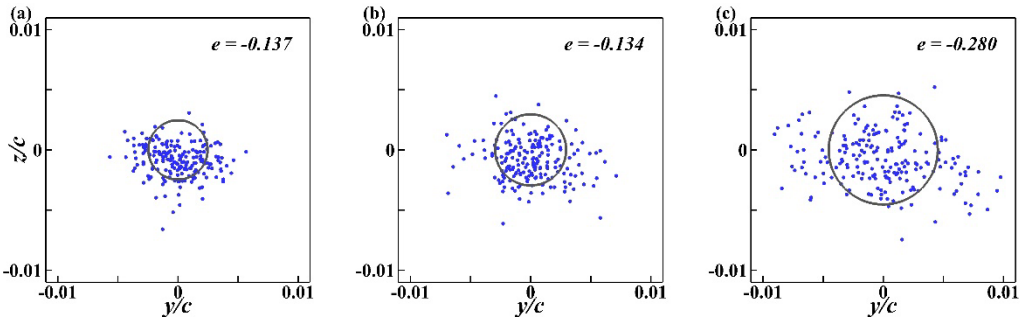

Fig. 2 Distribution of instantaneous vortex centers at the condition of *AoA* = 8°, U_∞ =20 m/s, with grey circle denoting the amplitude of wandering

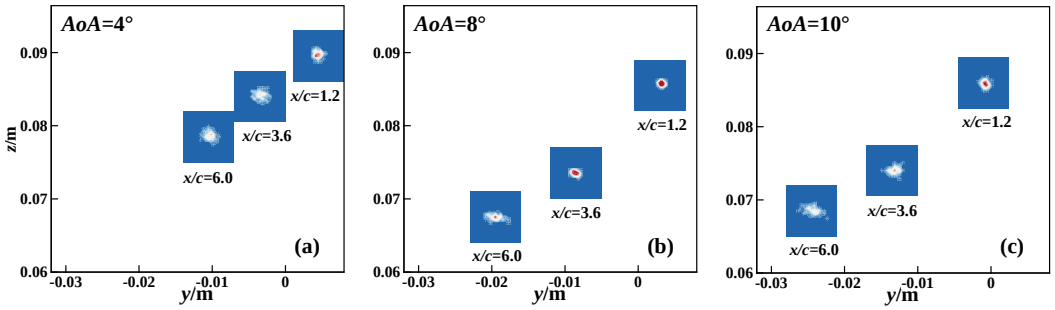

Fig. 3 Streamwise evolution of joint probability density distribution of vortex cores at *Re* = 2.8× 10^5 and different *AoA*, *x/c* = 1.2, 3.6, 6.0. The contour range is $[0.5\times10^5, 7.5\times10^5]$.

3 Wandering behavior of wingtip vortex

3.1 Instantaneous vortex centers of wingtip vortex

The instantaneous locations of wingtip vortex on each streamwise Stereo-PIV plane are computed to reveal the distribution of vortex centers. As can be observed in Fig. 2, the distribution of instantaneous vortex center develops from a nearly isotropic, collective pattern to an anisotropic and much more scattered pattern. The isotropic property of wandering motion is clearly seen in the near wake (*x/c* =1.2, Fig.2(a)) while anisotropy gradually take over as the vortex is transported into far wake (Fig.2(b) and Fig.2(c)). Moreover, the amplitude of wandering is amplified in streamwise direction, illustrated by the grey circle at the mean vortex center. By comparison of the correlation parameter of y_c and z_c of the vortex center, the fact that the wandering motion develops from isotropy to anisotropy is further corroborated.

In order to describe the evolution of wingtip vortex wandering along the streamwise direction more intuitively, joint probability density distribution function (j.p.d.f.) is calculated to characterize the magnitude of the vortex wandering in addition to its spatial distribution. It is found that the angle of attack has a great impact on the amplitude of wandering. The increase of the amplitude of wandering from *x/c* = 1.2 to 6.0 can be clearly observed at large *AoA* condition (8°, 10°), while at *AoA*=4°, the vortex center remains in a dispersive form degree of anisotropy is also increased, as is shown by the case at Re=2.8×10^5 in Fig.4. The Reynolds number has a weak

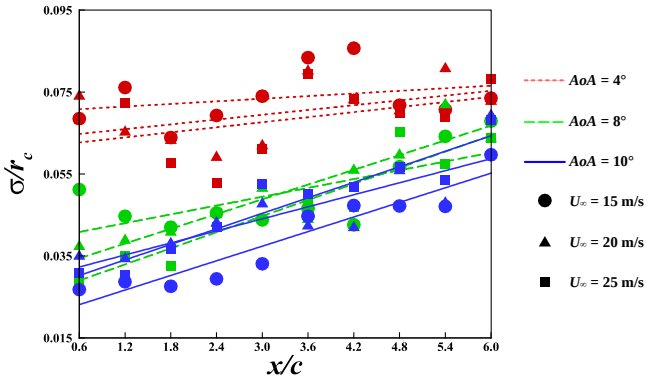

Fig. 4 Streamwise evolution of the amplitude of vortex wandering. The straight lines are the linear fit curves at each condition.

effect on the wingtip vortex wandering from 2.1×10^5 to 3.5×10^5 in the experimented conditions. Besides, it can be seen that the wingtip vortex undergoes an in-wash and up-wash trajectory as it is transported downstream.

3.2 Wandering amplitude of wingtip vortex

The amplitude of wandering is calculated in each experimental condition and streamwise section, and is non-dimensionalized by the core radius r_c. As can be seen in Fig.3, two major points can be observed: firstly, the amplitude of wandering is amplified in all conditions, in correspondence with the work by Beresh *et al.* [8]; secondly, the amplitude of wandering at larger *AoA* (8° and 10°) grows much more quickly along *x*-direction compared with small *AoA* (4°). The reason for such deviation is the difference in the stability of the wing tip vortex in different flow conditions, which is to be illustrated in detail in section 5.

4 Mechanism of wingtip vortex wandering

4.1 Linear stability analysis: methodology and code validation

Linear stability analysis linearizes small disturbances in a certain base flow during its onset and quantifies its temporal/spatial growth rate, perturbation frequency and modes of instability, which is suitable in the case of investigating the mechanism of vortex wandering, as such motion remains in a small disturbance scenario. In the present study, incompressible Navier-Stokes Equation is adopted in a cylindrical coordinate, and the parallel assumption is made which assumes zero derivatives in the basic state in *x*-direction so that a local LSA procedure qualifies [15]. The flow variable $\boldsymbol{q}=[u_r,\ u_\theta,\ u_x,\ p]^T$ is decomposed into a basic state $\bar{\boldsymbol{q}}(r)$ and a fluctuation component $\boldsymbol{q}'$. The fluctuation component $\boldsymbol{q}'$ is presumed to have a wave-like form which comprises the basis for the fluctuation, as defined in Eq. 2:

$$\boldsymbol{q}'(r,\theta,x,t)=[i\hat{u}_r,\hat{u}_\theta,\hat{u}_x,\hat{p}]^T\exp[i(\alpha x+n\theta-\omega t)]+\boldsymbol{c.c.} \tag{2}$$

in which α is the streamwise wavenumber, n is the azimuthal wavenumber, and ω is the frequency, with $\boldsymbol{c.c}$ being the conjugate complex. Herein, spatial LSA is performed to quantify the streamwise development of disturbances in the wingtip vortex flow. Therefore, the linearized N-S equation is rewritten as a polynomial eigenvalue problem $\boldsymbol{A}\hat{\boldsymbol{q}}=\alpha\boldsymbol{B}\hat{\boldsymbol{q}}$, with $\omega\in\mathrm{R}$, $\alpha=\alpha_r+i\alpha_i$ and $\hat{\boldsymbol{q}}=[i\hat{u}_r,\hat{u}_\theta,\hat{u}_x,\hat{p}]^T$

Table 1 Comparison of spatial stability results of Poiseuille flow in a pipe with literature

n	α, present method	α, Khorrami *et al.*,1989 [15]
0	0.519989251732426+ 0.020835493881362i	0.51998925171 + 0.020835493881i
1	0.535251083108396+ 0.017227643884052i	0.53525108 + 0.01722763i

Table 2 Comparison of spatial stability result of Batchelor vortex with literature

Re	α, present method	α, Parras *et al.*, 2007 [16]
667	0.365174487123736 - 0.222971346495823i	0.3651762873306434 - 0.2229717123848892i
10^8	0.246667715462097 - 0.001696062822232i	0.24666715 - 0.0016967876i

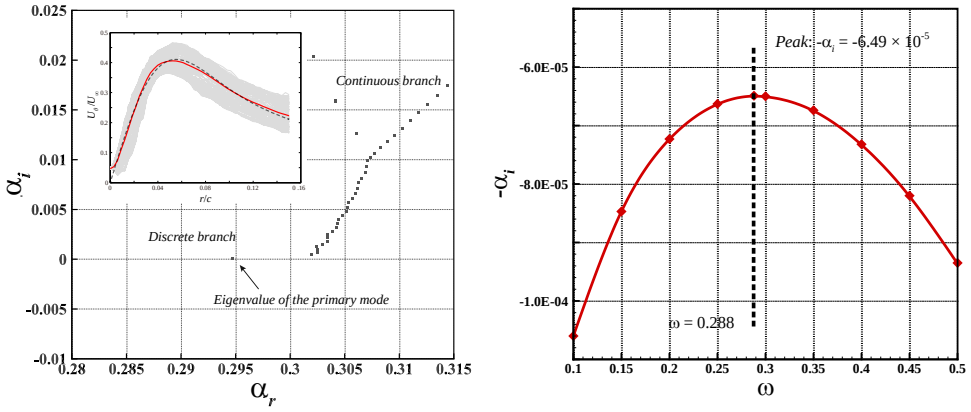

Fig. 5 Spatial linear stability result of the wingtip vortex at x/c = 5.4, AoA = 10°, U_∞ = 20 m/s: (a) eigenvalue spectrum: top-right inset being the azimuthally-averaged tangential velocity (red solid line) and its fitting curve (black dotted line), with grey area indicating azimuthal variation of tangential velocity, (b) stability curve at the same condition, dash line denoting the peak value and corresponding perturbation frequency ω.

being the eigenmode. The spatial growth rate of the corresponding eigenmode is quantified by $-\alpha_i$. The code is validated by four cases against literature which agrees well at least within five decimal places, as is shown in Table 1 and Table 2.

4.2 Linear stability analysis of the wingtip vortex

The linear stability analysis demands the base flow to be the accurate solution of Navier-Stokes equation. Therefore, the base flow of wingtip vortex is obtained by taking the time-averaged flow field of Stereo-PIV as a quasi-steady state and then fitting the canonical Batchelor vortex, which is an exact solution of N-S equation, to the experimental mean flow by least-square fit. The fitted result of the wingtip vortex at AoA = 10°, U_∞ = 20 m/s, x/c = 5.4 is illustrated in the inset of Fig. 5 (a). Then spatial LSA is performed upon the fitted base flow within a range of perturbation frequency ω. The azimuthal wavenumber n is set to -1, at which the disturbance is most amplified, as is reported in the work by Mayer *et al.* [11], Fabre *et al.* [12], Parres *et al.* [16]. For each ω, an eigenvalue spectrum is calculated, which consists of a discrete branch where eigenmodes are confined in the shear layer and

Fig. 6 Streamwise variation of spatial growth rate of disturbance by linear stability analysis

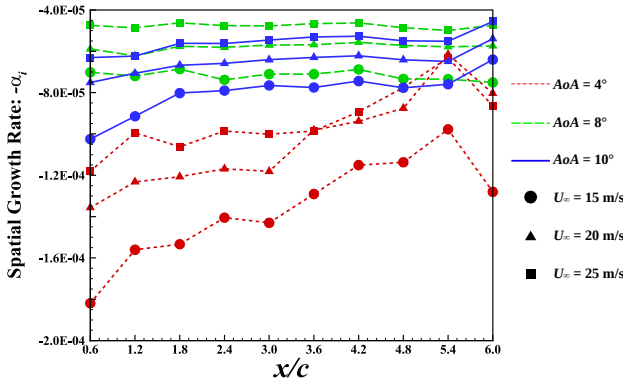

a continuous branch which describes freestream oscillations [14], as can be seen in the stability result in Fig. 5(a). The single eigenvalue located near $\alpha_i = 0$, with the largest spatial growth rate denotes the primary mode at the corresponding ω. Then the stability curve is obtained by a frequency sweep, which yields the least stable eigenmode of the base flow with its growth rate and perturbation frequency (see Fig. 5(b)). The spatial linear stability analysis is performed for each condition and streamwise location in the experiment.

4.2 Evolution of instability of wingtip vortex

The spatial growth rate of the most unstable eigenmode of the wingtip vortex at each experimental condition is illustrated in Fig. 6. The results indicate that all the wingtip vortex measured in the experiment remains marginally stable in the wake region of *x/c*=0.6-6.0, which in turn explains the fact that the wingtip vortex does not breakdown within the region of observation. Another important fact is that the spatial growth rate at large *AoA* condition (8°, 10°) exceeds that at smaller *AoA* (4°) by a large margin almost in the entire wake region, which implies that disturbance tends to amplify much quicker in a wingtip vortex with larger circulation (larger *AoA*). This stability result accounts for the phenomenon described in section 3.2 that the amplitude of wandering at larger *AoA* (8° and 10°) grows at a much larger rate along streamwise direction compared with small *AoA* (4°), for the reason that the wingtip vortex at larger *AoA* is relatively more unstable with fast-amplifying disturbances.

4.3 Analysis of the mechanism of wingtip vortex wandering

The relation between the intensifying of the wandering motion and vortex instability has been explained in section 4.2. To reveal the underlying mechanism of vortex wandering, the most unstable spatial modes at different experimental conditions are solved, which correspond to the eigenfunction $\hat{\boldsymbol{q}} = [i\hat{u}_r, \hat{u}_\theta, \hat{u}_x, \hat{p}]^T$ of the most unstable eigenvalue $\alpha = \alpha_r + i\alpha_i$. The least-stable eigenmode of the wingtip vortex at *AoA*=8°, U_∞=20m/s, *x/c*=6.0 is shown in Fig. 7. It can be observed that the amplitude of crosswise disturbance $\hat{u}_r, \hat{u}_\theta$ is far more intense than that of streamwise disturbance $\hat{u}_x$, which might be the driven factor of the crosswise displacement of vortex center, leading to the wandering motion. In addition, all components of the disturbance basically are confined in the core region. The boundary of vortex core is illustrated by the vertical dash line.

Fig. 8 Disturbance mode $\hat{q}(r)$ of spatial instability at *AoA* = 8°, U_∞ = 20m/s, *x/c* = 6.0, dashed vertical line indicating the location of maximum tangential velocity of the corresponding wingtip vortex

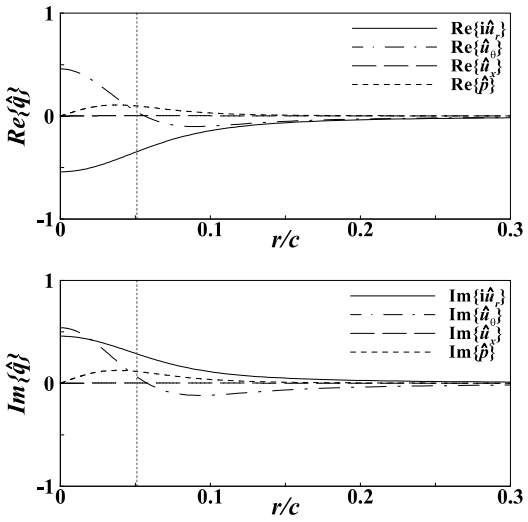

Fig. 7 2-dimensional distribution of the disturbance mode of wingtip vortex at *AoA*=8°, U_∞=20m/s, *x/c*=6.0. The upper-left frame displays the relative scale of the time-averaged base flow, for comparison of the disturbance mode

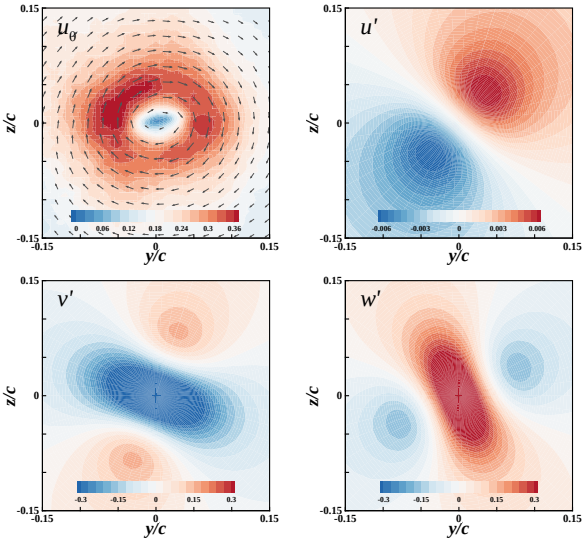

To further uncover the 2-dimensional distribution of the disturbance mode, the phase function is also taken into consideration to demonstrate the azimuthal distribution, with temporal dimension frozen at t = 0. The result at the same condition of *AoA*=10°, U_∞=20m/s, *x/c*=6.0 is shown in Fig. 8. As can be observed, the crosswise velocity perturbation v', w' is much stronger than the two-lobe-shaped streamwise velocity perturbation u'. Moreover, the extremum of the crosswise velocity perturbation locates at the vortex center, which further corroborate the role played by v', w' in displacing the vortex. The tangential velocity of the base flow is also included to demonstrate the relative scale of the disturbance mode compared to the base flow. Last but not least, the temporal periodicity of the disturbance mode is then taken into account, and the crosswise velocity perturbation v', w' are composed into a resultant crosswise perturbation u'_{cr}. As is illustrated in Fig. 9, u'_{cr} is fully centralized and directed at the vortex center with a maximum. As time advances, u'_{cr} rotates itself clockwise. This directed velocity perturbation at the core continues offsetting the vortex, causing the entire vortex to wander (Fig. 9(a)). The

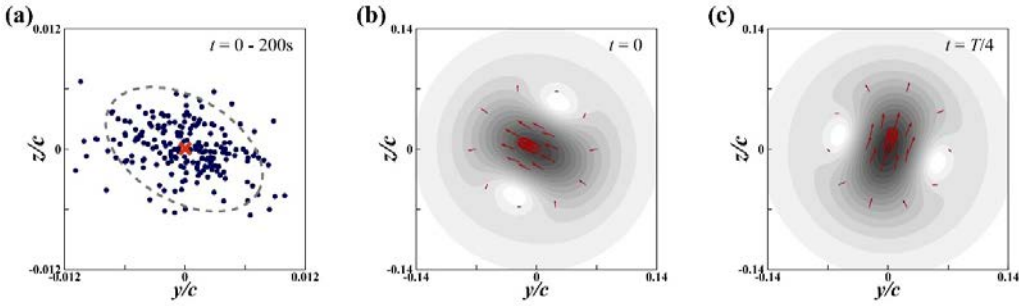

Fig. 9 Comparison between experimental instantaneous vortex core distribution and disturbance mode by LSA: (a) Instantaneous vortex core distribution at AoA=10°, U_∞=20m/s, x/c=6.0, with red cross and dashed oval denoting the mean vortex center and the anisotropic pattern, (b)(c) Distribution of crosswise perturbation velocity at t = 0 and t = T/4.

periodicity and directivity of the crosswise velocity perturbation force the vortex to wander about its center, which is the underlying mechanism of wingtip vortex wandering.

6 Conclusion

In this paper, the wandering behavior of the wingtip vortex generated by a NACA0012 rectangular wing at AoA = 4°, 8°, 10°, and Re = 2.1×10^5, 2.8×10^5, 3.5×10^5 is observed by Stereo-PIV experiment in detail, which focuses on its streamwise development from x/c = 0.6 – 6.0. It is discovered that the distribution of instantaneous vortex center transits to an anisotropic pattern in the far-wake. The amplitude of vortex wandering increases in the streamwise direction in all conditions, but at a significantly larger amplification rate at large AoA conditions. This phenomenon is further investigated by spatial linear stability analysis, where a local LSA procedure is taken, to reveal the mechanism underlying the spatial development of vortex wandering. The stability result yields an evidently larger spatial growth rate of disturbance at the condition of large AoA, which explains the distinct characteristics of the spatial development of vortex wandering at different AoA conditions. The wingtip vortex is also found to be less stable at larger Reynolds number. Furthermore, the 2-dimensional disturbance mode of the wingtip vortex measured in the Stereo-PIV is obtained at each experimental condition. The crosswise and time-dependent distribution of the velocity perturbation uncovers a centralized velocity perturbation at the vortex center, which rotates periodically about the vortex center, offsetting the entire vortex. Such mechanism leads to the wandering behavior of wingtip vortex observed in the experiment. Still, there are some questions remaining open, such as the anisotropic distribution of instantaneous vortex center and the origin of this unique pattern of velocity perturbation, which will be further investigated in detail in future work.

References

1. BIRCH D, LEE T. Structure and Induced Drag of a Tip Vortex[J]. Journal of Aircraft, 2004, 41(5): 1138-1145.

2. GERZ T, HOLZÄPFEL F, DARRACQ D. Commercial aircraft wake vortices[J]. Progress in Aerospace Sciences, 2002, 38(3): 181–208.
3. LEIBOVICH S. Vortex stability and breakdown - Survey and extension[J]. AIAA Journal, 1984, 22(9): 1192–1206.
4. EDSTRAND A M, DAVIS T B, SCHMID P J, et al. On the mechanism of trailing vortex wandering[J]. Journal of Fluid Mechanics, 2016, 806(R1): 1–11
5. S.C.C. BAILEY, S. TAVOULARIS. Measurements of the velocity field of a wing-tip vortex, wandering in grid turbulence[J]. J. Fluid Mech., 2008, 601(2008): 281–315.
6. DEVENPORT W J, RIFE M C, LIAPIS S I, et al. The structure and development of a wing-tip vortex[J]. Journal of Fluid Mechanics
7. DEEM E, EDSTRAND A, REGER R et al. Deconvolution Correction for Wandering in Wingtip Vortex Flowfield Data[J]. Journal of Fluid Science and Technology, 2013, 8(2): 219–232.
8. BERESH S J, F. HENFLING J, SPILLERS R W. Meander of a fin trailing vortex and the origin of its turbulence[J]. Experiments in Fluids, 2010, 49: 599–611.
9. HEYES A L, JONES R F, SMITH D A R. Wandering of wing-tip vortices[C]//Proceedings of the 12th International Symposium on Application of Lase Techniques to Fluid Mechanics. 2004, 22(9): 1192–1206.
10. THEOFILIS V. Advances in global linear instability analysis of nonparallel and three-dimensional flows[J]. Progress in Aerospace Sciences, 2003, 39: 249–315.
11. MAYER E W, POWELL K G. Viscous and inviscid instabilities of a trailing vortex[J]. Journal of Fluid Mechanics, 1992, 245:91-114.
12. FABRE D, JACQUIN L. Viscous instabilities in trailing vortices at large swirl numbers[J]. Journal of Fluid Mechanics, 2004, 500(500): 239–262.
13. OBERLEITHNER K, SIEBER M, NAYERI C N, et al. Three-dimensional coherent structures in a swirling jet undergoing vortex breakdown: stability analysis and empirical mode construction[J]. Journal of Fluid Mechanics, 2011, 679: 383–414.
14. EDSTRAND A M, SCHMID P J, TAIRA K. A parallel stability analysis of a trailing vortex wake[J]. Journal of Fluid Mechanics, 2018: 858–895.
15. KHORRAMI R M, ASH R L. Application of Spectral Collocation Techniques to the Stability of Swirling Flows[J]. Journal of Computational Physics, 1989, 81: 206–229.
16. PARRAS L, FERNANDES-FERIA R. Spatial stability and the onset of absolute instability of Batchelor's vortex for high swirl numbers[J]. Journal of Fluid Mechanics, 2006, 583: 27–43.